ADVANCED OPTICAL MATERIALS
www.advopticalmat.de

Photon-Correlation Studies on Multichromophore Macrocycles of Perylene Dyes

Ulrich Müller, Peter Spenst, Philipp Kagerer, Matthias Stolte, Frank Würthner, and Jens Pflaum**

Dedicated to Professor Jochen Feldmann on the occasion of his 60th birthday

Organic dyes offer unique properties for their application as room temperature single photon emitters. By means of photon-correlation, the emission characteristics of macrocyclic *para*-xylylene linked perylene bisimide (PBI) trimers and tetramers dispersed in polymethyl methacrylate matrices are analyzed. The optical data indicate that, despite of the strong emission enhancement of PBI trimers and tetramers according to their larger number of chromophores, the photon-correlation statistics still obeys that of single photon emitters. Moreover, driving PBI trimers and tetramers at higher excitation powers, saturated emission behavior for monomers is found while macrocycle emission is still far-off saturation but shows enhanced fluctuations. This observation is attributed to fast singlet–singlet annihilation, i.e., faster than the radiative lifetime of the excited S_1 state, and the enlarged number of conformational arrangements of multichromophores in the polymeric host. Finally, embedding trimeric PBI macrocycles in active organic light-emitting diode matrices, electrically driven bright fluorescence together with an indication for antibunching at room temperature can be detected. This, so far, has only been observed for phosphorescent emitters that feature much longer lifetimes of the excited states and, thus, smaller radiative recombination rates. The results are discussed in the context of possible effects on the $g^{(2)}$ behavior of molecular emitters.

1. Introduction

The use of molecular emitters as single photon sources is of great interest due to their large oscillator strength, Lambertian emission characteristics and high radiative emission rates in combination with color tunability over a wide spectral range. The latter can be accomplished varying either the size or spatial distribution of the π-conjugated electron system by, e.g., chemical functionalization with suited so-called auxochrome substituents. Besides, the binding energy of the excited electron-hole pair which usually is of Frenkel-type character can obtain values as large as 1 eV and, hence, promises single photon source operation even at room temperature, a range that is still far off for inorganic semiconductor quantum systems.[1–3] However, while molecular layers of aggregated dyes and semiconducting polymers by virtue of their versatile optical and opto-electronic properties have successfully entered the market of organic light-emitting diodes (OLEDs) and displays and have even reached commercial competitiveness, the implementation of organic molecules in electrically driven single photon sources still poses a challenge and demands for innovative material concepts.[4–6] One of the drawbacks using molecular emitters is their lower photostability in comparison to inorganic quantum dots or atomic defects in crystalline lattices, such as NV centers in diamond or silicon vacancies in SiC.[7,8] However, by minimizing oxygen exposure during preparation and optimizing excitation schemes, an overall amount of up to 10^{11} photons per lifecycle can be achieved for a molecular guest emitter, already.[9] A second major problems to solve is the spin-dependent recombination dynamics of injected electrons and holes. As 75% of the injected electron-hole pairs form an excited triplet state of total spin 1, its recombination to the singlet S_0 ground state becomes dipole forbidden and, thus, results in a long-living dark state. Residing in this dark state with lifetimes of up to several µs or even ms spoils the otherwise highly efficient radiative recombination with typical rates of 10^9 s^{-1} for fluorescent emitters. Accordingly, the bottleneck of triplet state formation and its impact on the efficiency of single photon emitters have to be minimized or circumvented. One possible solution has been established by phosphorescent emitters which by their strong spin-orbit coupling exhibit a mixing of spin and orbital angular momentum and, thereby, can lift the restriction imposed by dipole selection rules.[10,11] However, the radiative depletion of their triplet state comes at the expenses of rather modest recombination rates in the range of 10^6 s^{-1}, i.e., usually being three orders of magnitude smaller than those of fluorescent emitters.[12] This recombination efficiency is somewhat comparable to TADF (thermally activated delayed fluorescence)

U. Müller, P. Kagerer, J. Pflaum
Lehrstuhl für Experimentelle Physik VI
Universität Würzburg
Am Hubland, 97074 Würzburg, Germany
E-mail: jpflaum@physik.uni-wuerzburg.de
P. Spenst, M. Stolte, F. Würthner
Institut für Organische Chemie and Center for Nanosystems Chemistry
Universität Würzburg
Am Hubland, 97074 Würzburg, Germany
E-mail: wuerthner@uni-wuerzburg.de
The ORCID identification number(s) for the author(s) of this article can be found under https://doi.org/10.1002/adom.202200234.

DOI: 10.1002/adom.202200234

emitters which, in fact, show fluorescence but delayed by a thermally activated reverse intersystem crossing from the excited triplet T_1 to the singlet S_1 state, both lying close by in energy.[13,14]

Here, we elucidate the potential of multichromophore macrocyclic molecular emitters that were recently developed in our laboratory.[15] As we will show such macrocyclic dye architectures offer additional excitation and relaxation pathways by their interlinked dyes which enable single photon emission and, thus, promote them as interesting candidates for efficient, fluorescent based nonclassical light sources.

For our studies we chose perylene bisimide (PBI) dyes that are among the few chromophores that reach fluorescence quantum yields > 99%, thereby being characterized by very low rates for internal conversion to the ground state and intersystem crossing into triplet states. In combination with their exceptional chemical and photostability, this has rendered these compounds highly interesting for technological applications as well as fundamental studies on their photon statistics. While our research is devoted to newly developed macrocyclic oligomeric architectures bearing up to four perylene bisimide (PBI) dyes, we like to advert the reader to earlier single molecule spectroscopy studies on individual PBIs[16–18] as well as linear,[19–21] macrocyclic[22] or dendritic[23–28] PBI oligomers. For these studies it was also beneficial that the absorption and emission maxima of PBIs are tunable over a significant spectral range from green to red by appropriate substituents at the PBI core positions (labeled with X in **Figure 1**a).[29,30] Here, for our purpose phenoxy substituents were most appropriate that are known to shift the emission maxima to values of about 600 nm, afford high solubility and show little propensity for aggregation.[31] For the current study it is furthermore most advantageous that the substituents in imide positions (labeled R in Figure 1a) have little impact on the optical properties of these dyes and do not provide through-bond coupling between them with the utilized *para*-xylylene spacer groups. Compared to linear and dendritic architectures, macrocyclic architectures have furthermore the advantage of including dyes of identical structure and energy levels at least for their time-averaged high-symmetry structures observed by, e.g., proton NMR spectroscopy.[32]

For the PBI dyes chosen in this study we have previously reported the steady-state and time-resolved optical properties. Accordingly, fluorescence quantum yields in toluene solution are 0.86 for monomeric **1PBI**, 0.79 for trimeric macrocycle **3PBI** but only 0.16 for tetrameric macrocycle **4PBI**. While the former values showed little change in dichloromethane, for the latter a significant increase was observed with a value of 0.53. This behavior could be attributed to the nonrigid character of **4PBI** that can accommodate either a ring-type structure with less interacting PBI dyes (prevailing in dichloromethane) or a folded structure with pairwise aggregated dyes (prevailing in toluene).[14] We exclude the dimer species from this work, which has also been synthesized and extensively studied, as the co-planar arrangement of its chromophores affords a cavity that is prone to embed all kinds of planar aromatic guest molecules that, in turn, can strongly influence the excited state properties.[33,34]

2. Results and Discussions

2.1. Photon-Correlation Method

The following studies on the photophysical properties and correlation statistics on *para*-xylylene linked **3PBI** trimers and **4PBI** tetramers are carried out in comparison to **1PBI** monomers

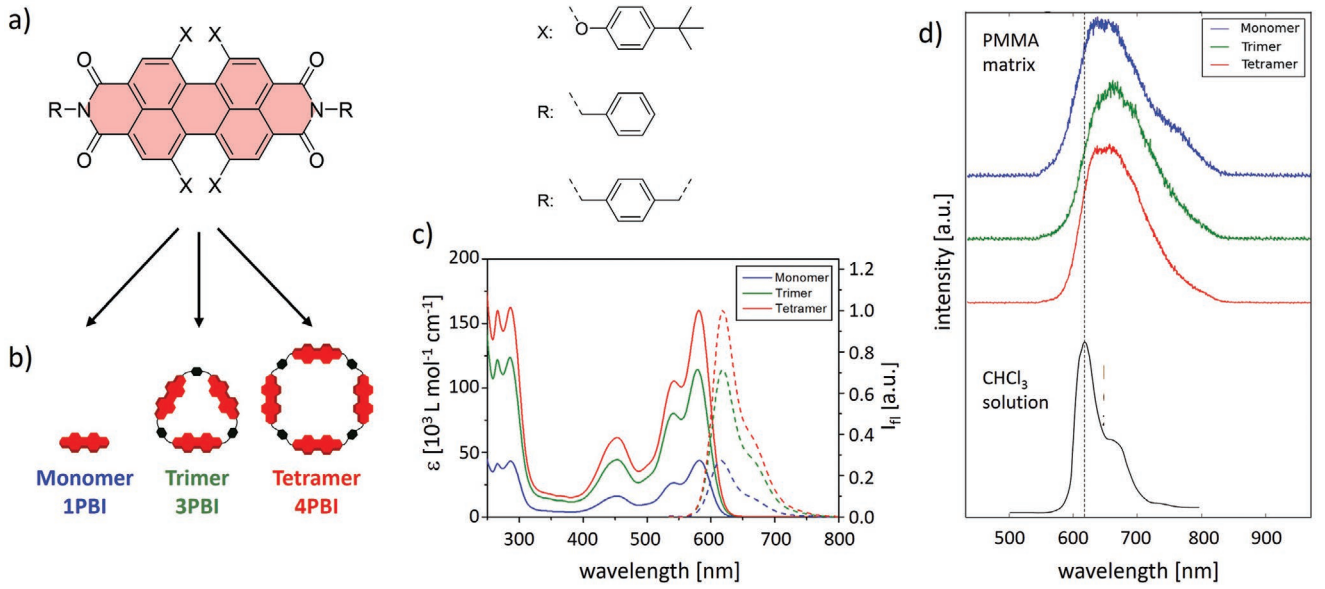

Figure 1. a) Molecular structures of the perylene bisimide (PBI) monomer compound with benzyl substituents (**1PBI**). b) Schematic representation of PBI monomer and (multi-)chromophore macrocycles bearing three (3PBI) or four (4PBI) dyes. c) Room temperature absorption (straight lines) and emission (dashed lines) spectra of PBI monomer, trimer and tetramer dissolved in $CHCl_3$ (5×10^{-6} M). Absorption and emission intensities scale with the number of PBI chromophores and, thus, molecular dipole moments, hinting at the weak electronic coupling between the individual dyes. d) PBI monomer, trimer and tetramer single molecule spectra, measured in doped polymethyl methacrylate (PMMA) matrices (top). The doping concentration of 10^{-8} wt% yields an average in-plane molecular spacing of 1.5 µm in the 100 nm thick PMMA films. For comparison, the tetramer emission in $CHCl_3$ solution is shown.

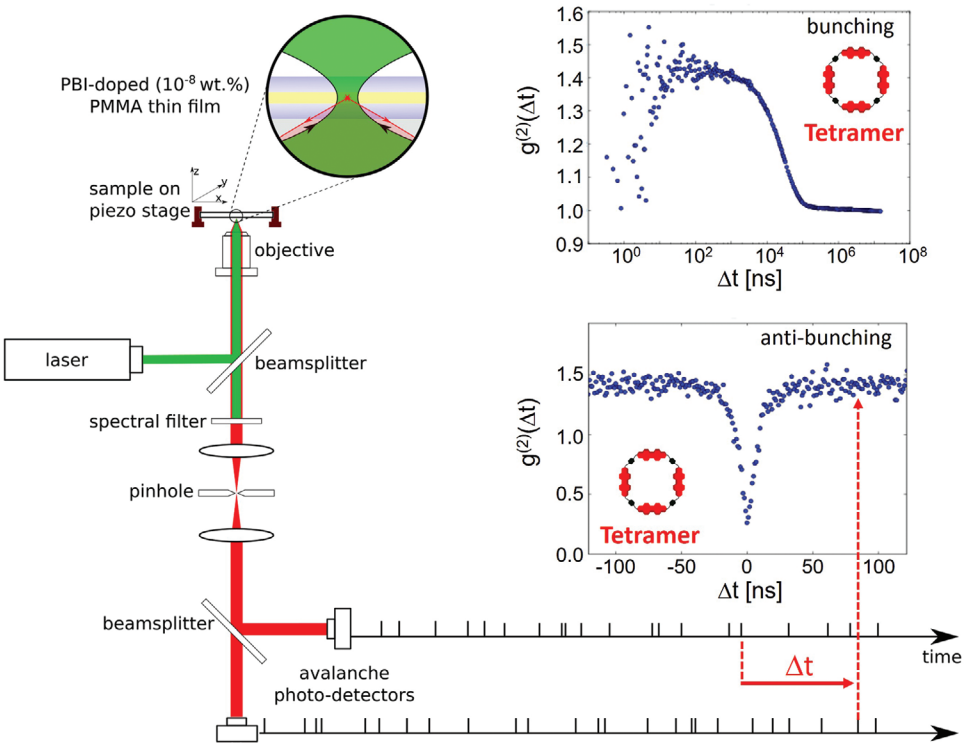

Figure 2. Photon-correlation measurements by a Hanbury–Brown Twiss setup consisting of a 50:50 beam splitter and two avalanche photodetectors. Intercorrelating the delays between different events in both channels, the $g^{(2)}$ function can be calculated, which contains information on the nature of the emitter and on the dynamics of the emission process. If the focal spot contains just one single emitter, the $g^{(2)}$ function exhibits a dip and approaches zero for zero time delay (antibunching, lower graph). In the presence of long-lived dark state, the distribution shows a step at long delay times (bunching, upper graph).

as reference. Before presenting the experimental findings and their interpretation, we briefly highlight the main aspects of the photon-correlation technique, its experimental implementation is illustrated in **Figure 2**. Photon correlation measurements were performed by confocal microscopy combined with a Hanbury–Brown Twiss setup. The latter consists of two single photon avalanche diodes positioned in each path of a 50:50 beam splitter. By use of two photon detectors instead of just one, we avoid effects by the deadtime (≈24 ns) and after-pulsing of the detectors yielding a time resolution below 350 ps. During the measurements, each photodiode continuously marks the incident photons by defined time stamps. The delay times Δt between all events in both channels are estimated and yield a probability distribution as function of delay. The second order correlation function, $g^{(2)}$, which is defined by the ratio of expectation values for the intensity products at time t and $t + \Delta t$ normalized to the square of the expectation value of the intensity at time t reads

$$g^{(2)}(\Delta t) = \frac{\langle I(t) \cdot I(t+\Delta t) \rangle}{\langle I(t) \rangle^2} \quad (1)$$

and contains information on the probability of detecting a second photon at time $t + \Delta t$ if the first photon has hit the other detector at time t. Relevant for our studies, in the presence of a single photon emitter, $g^{(2)}$ approaches zero at zero time delay (antibunching, see lower inset in Figure 2). Describing the intensity by the Fock states of the electric field and applying second quantization, the anticorrelation function can be referred to a particle number basis

$$g^{(2)}(0) = 1 - \frac{1}{N} \quad (2)$$

where N is the number of photons simultaneously entering the Hanbury–Brown Twiss setup.[7]

This gives the strong criterion at hand that $g^{(2)}(0)$ has to be < 0.5 for a single photon emitter. Moreover, at larger time scales the $g^{(2)}$ function might show bunching (upper inset of Figure 2) which contains information on long-living dark states, such as triplets, populated by inter-system crossing and governing the excitation dynamics in this time regime.

2.2. Absorption and Emission Characteristics

The *para*-xylylene linker is expected to yield a weak though present interaction between neighboring chromophores which will become obvious in the presentation of **3PBI** and **4PBI** optical properties. For instance, upon weak excitation the spectral positions of absorption and emissions in solution are independent of the number of PBI dyes whereas their respective absorption and emission strengths scale linearly with the number of chromophores, Figure 1c. This indicates the covalent linkage of chromophores to leave the quantum efficiency essentially unchanged making the macrocycle concept highly attractive for

opto-electronic applications. For comparison, Figure 1d displays the single molecule emission spectra of PBI monomers, trimers and tetramers doped in PMMA at a concentration of 10^{-8} wt%. As can be seen in relation to the **4PBI** reference spectra measured in chloroform ($CHCl_3$), the single molecule emission in solid state PMMA matrices occurs in the same wavelength range but appears to be more structureless and redshifted. We attribute this redshifted emission of PBI macrocycles in PMMA to a more pronounced conformational heterogeneity compared to $CHCl_3$ solution. This involves in particular the conformation of the tetraphenoxy groups with regard to the rigid perylene bisimide scaffold that has been shown to have a major impact on the absorption and fluorescence maxima.[31,35] Local matrix effects become also evident by slight variations in the spectral emission for one and the same PBI compound at different locations in the sample. Yet, the similar emission characteristics of **1PBI** monomer, and **3PBI** and **4PBI** macrocycles justify their comparative analysis in the further investigations.[36]

2.3. Single Molecule Photoluminescence Studies

We start our photon correlation studies on PBI monomers and multichromophores with an analysis of their single molecule emission properties in PMMA thin film matrices doped by **1PBI**, **3PBI**, and **4PBI** at a concentration level of 10^{-8} wt.%. Concerning the molar masses of PMMA (3.5×10^5 g mol^{-1}) and PBI monomer (about 10^3 g mol^{-1}, and accordingly higher for PBI trimer and tetramer), this doping concentration relates to a mean of one PBI emitter in the confocal detection volume (about 0.1 µm^3). The probability of detecting just one molecule is further enhanced by PMMA layer thicknesses of just 100 nm, i.e., more than one order of magnitude thinner than the vertical extension of our detection spot, which translates into a mean in-plane molecular spacing of about 1.5 µm. To distinguish the case of a single emitter from that of multiple emitters in the detection volume, the value of the respective anticorrelation function at $\Delta t = 0$, i.e., $g^{(2)}(0) > 0.5$ versus $g^{(2)}(0) < 0.5$, has been considered a first criterion. **Figure 3** presents representative photoluminescence (PL) intensity maps of the three different PBI compounds in PMMA. Bright spots indicating the position of individual or multiple molecules are homogenously distributed across the matrix and exhibit count rates of up to 80 cts ms^{-1} at 1 µW excitation power. The corresponding emission spectra are displayed in Figure 1d and show a rather featureless but spectrally identical intensity distribution. The high count rates achieved already at small or modest excitation powers promise an efficient estimation of the corresponding anticorrelation function before irreversible photobleaching of the molecules. The latter was determined by time trace measurements to last for several minutes up to one hour under constant illumination. Even though this demonstrates the high photostability of PBI monomers and macrocycles, it should be kept in mind that for the determination of the antibunching of a fluorescent emitter with nanosecond radiative lifetime it needs about 10^6 times more photons than for a phosphorescent emitter. The measured $g^{(2)}$ functions for each of the three different PBI derivatives are plotted in the lower row of Figure 3. All correlation curves show a pronounced antibunching with $g^{(2)}(0)$ being clearly located below 0.5 (dotted horizontal line), demonstrating the single photon emitter character of each of the PBI compounds and, thus, their suitability for application in nonclassical light sources. It is important to note here that the single photon emission observed for **3PBI** and **4PBI** implies

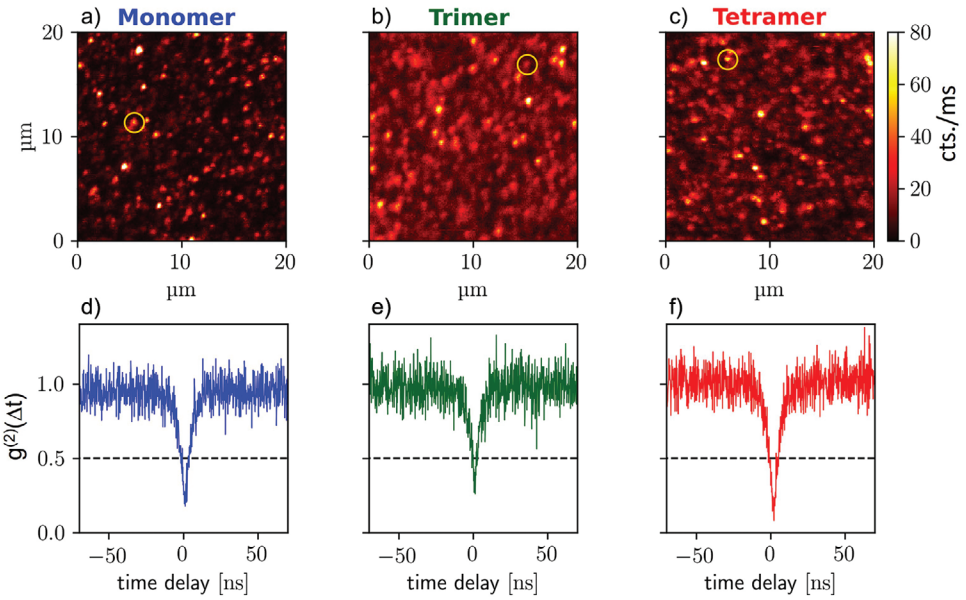

Figure 3. Photoluminescence intensity maps recorded on a) **1PBI** monomer and b) **3PBI** and c) **4PBI** macrocycles dispersed in PMMA at the single molecule level. Colors coded photon counting rates are indicated by the scale. The corresponding $g^{(2)}(\Delta t)$ correlation functions for d) monomer, e) trimer, and f) tetramer macrocycle measured on the encircled spots in the upper PL maps, respectively, are displayed in the row below. As indicated by the $g^{(2)}(\Delta t) < 0.5$ behavior for $\Delta t \to 0$, the anticorrelation functions of PBI monomer, trimer, and tetramer confirm that of a single photon emitter. All measurements were carried out at 532 nm excitation wavelength and 1 µW excitation power.

that the *para*-xylylene mediated interaction is still sufficient to quench possible multiple excitonic states by either singlet-singlet or singlet-triplet annihilation processes on times scales faster than the radiative S_1 decay. Similar processes have been reported for other multichromophores in solid state matrices and aggregates.[24,37] The S_1 decay, responsible for the emission, can be deduced by the full width at half maximum (FWHM) of the individual dips, which at weak excitation (see Equation 3) is a measure for the sum of radiative and nonradiative decay rates, FWHM = 2 ln(2) / (k_r + k_{nr}),[14,41] and yields radiative lifetimes between 2.5 and 4.5 ns for the PBI compounds. These lifetimes resemble those attributed by fs transient absorption spectroscopy to the $S_1 \rightarrow S_0$ decay of PBI macrocycles in toluene and are referred to the same decay in our PBI-doped PMMA matrices.[15]

As will be addressed in the discussion of the bunching data below, the similar FWHM for the three PBI compounds of different chromophore number and absorption strength (Figure 1c) indicates that k_r is still the dominating rate, i.e., no other nonradiative relaxation channel contributes to the decay at this low excitation powers of 1 µW, and that the assumption of a simple three-level excitation scheme does not hold for **3PBI** and **4PBI** as otherwise, the ultrafast annihilations processes should significantly affect k_{nr} and, thus, the observed lifetimes.

2.4. Photon Antibunching Experiments

To elucidate this behavior further, the antibunching width has been analyzed in a wide range of excitation powers. Illustrated by **Figure 4**a, for excitation powers up to 10 µW, no distinct variation in the respective lifetimes for **1PBI** and **4PBI** appear. Only the **3PBI** trimer shows a certain lifetime shortening at small powers below 1 µW (green line) which might originate from either photo- or thermally-induced release of steric hindrance imposed by the local environment. Yet, this variation occurs within the lifetime interval mentioned above and vanishes for excitation powers above 1 µW.

Another peculiarity can be observed in the power-dependent antibunching width of the **4PBI** tetramer. For this macrocycle we can distinguish a distinct upper and lower boundary of antibunching widths, i.e., lifetime data, as well as bunching times (see discussion below). Accordingly, our single molecule experiments clearly corroborate the existence of different conformational states which have been recently suggested as explanation for rather different fluorescence quantum yields and life times for **4PBI** in different solvents.[15] Thus, the observed differences in the (averaged) steady-state and time-resolved spectroscopies can be unambiguously related to different chromophore configurations with the open ring conformation (as shown in Figure 1b) and the folded structure with more strongly interacting PBI dye pairs but also to changes in the mutual chromophore interaction defining the two border cases. Indeed, the photophysical properties of the tetramer are expected to be very sensitive on the respective conformational arrangement of the chromophores within the macrocycle and, thus, on the local environment. This is corroborated by the fact that even within the lifecycle of the emitters we sometimes observe spectral jumps in the emission accompanied by changes in the related correlation properties, an optical behavior reported also for many other chromophores in solid state matrices.[38] Hence, it appears difficult to exactly assign one of the two border configurations (open vs closed cycle) to either of the two **4PBI** antibunching widths shown in Figure 4a.

Aiming for the emission characteristics of the three PBI species at even higher excitation power above saturation, i.e., where

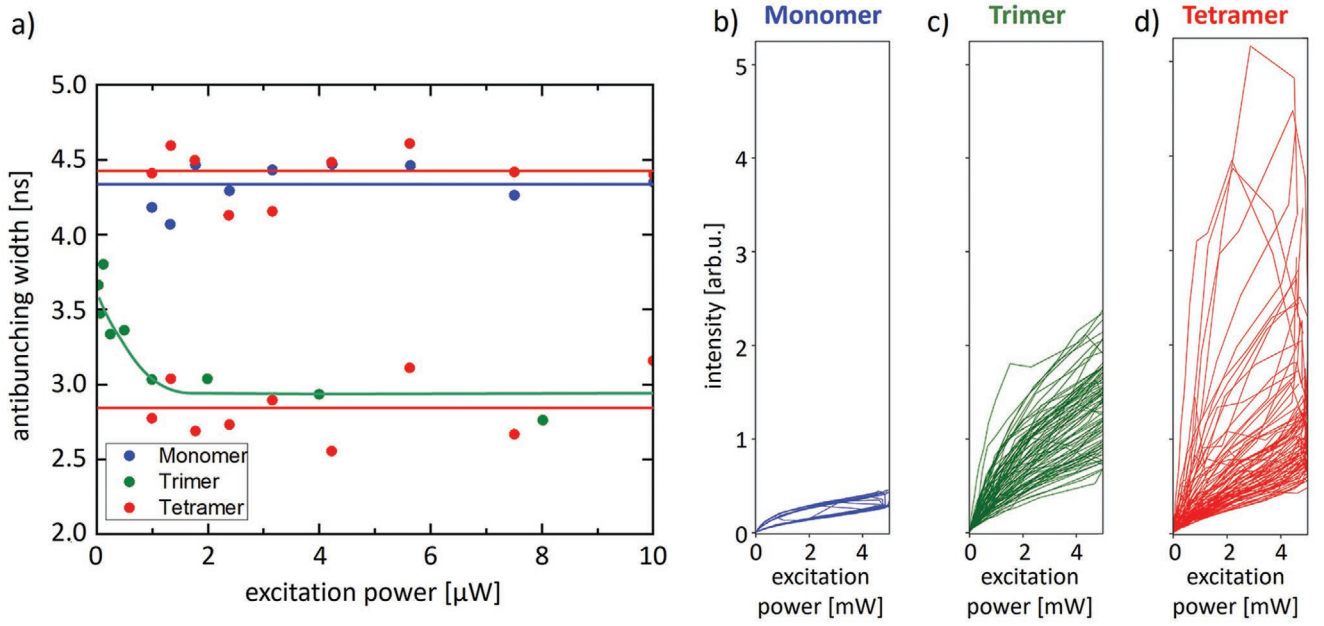

Figure 4. a) Width of the antibunching (see Figure 3d–f), for **1PBI**, **3PBI**, and **4PBI** as function of excitation power. Here, the widths for both tetramer configurations observed in the experiment are shown (see the text). Indicated by guide-to-the eyes, the deduced lifetimes of 2.5–4.5 ns for the radiative singlet state stay almost constant up to excitation powers of 10 µW. The relative PL intensity at much stronger excitation power up to 4 mW is shown for **1PBI**, **3PBI**, and **4PBI** in (b)–(d), respectively. All data recorded within one cycle are connected by straight lines.

the absorption rate equals the S_1 decay rate, we observed the behavior shown in Figure 4b–d. In this experimental configuration the excitation power was cycled at a rate of 4 Hz between 0 to 4 mW by means of a rotating neutral density filter. As can be seen by the data (points connected by straight lines refer to the same excitation cycle), the PBI monomer shows two distinct PL branches which smoothly increase with power. The lower one refers to the monomer dark state and, thus, represents the power-dependent background emission which scales linearly with excitation power. The upper branch refers to the bright state fluorescence of the molecule plus background emission. Hence, the difference between upper and lower branch corresponds to the neat emission of the PBI monomer's bright state and, as can be seen, becomes independent of excitation power. This behavior resembles a three-level excitation scheme comprising a singlet ground- and excited as well as a long-living dark state which limits the photodynamics at high powers.

In contrast, the behavior for **3PBI** as well as **4PBI** appears to be far-off saturation and shows strong fluctuations in photoluminescence with increasing excitation power. Furthermore, at a given power the fluctuation amplitude is larger for macrocycles hosting a larger number of chromophores. These observations lead to the following conclusion that upon strong excitation, **3PBI** and **4PBI** species neither occupy a saturated fluorescent state nor a completely dark state. Moreover, as the fluorescent enhancement for **3PBI** trimers and **4PBI** tetramers at strong excitation is even larger as one would expect simply by the number of chromophores (with the monomer as reference), additional processes have to support photon emission in this power regime. By virtue of the µs triplet lifetime (see discussion of bunching below), triplet-triplet annihilation is expected to be the most efficient mechanism, but also singlet-triplet annihilation might contribute a substantial part to the observed PL enhancement. Similar recombination schemes have been proposed in case of multiperyleneimide substituted polyphenylene dendrimers.[23] Complementary, both channels would be responsible for the emerging fluctuations at high powers as the efficiency of annihilation is sensitive to the mutual orientation of the chromophores hosting the two excited states. An incremental number of chromophores should thus lead to a higher susceptibility on the configurational degrees of freedom and should result in an overall larger variation of triplet-triplet or singlet-triplet annihilation efficiency which, ultimately, will lead to larger fluctuations of the fluorescence.

Finally, before discussing devices based on PBI macrocycles, we will examine the bunching behavior of the various PBI macrocycles in respect to that of the monomer at larger time delays.

Figure 5 presents a compilation of the bunching characteristics of **1PBI** and, representatively, **4PBI** as function of time and power. First, the characteristic bunching step occurs at delay times of about 10^{-6} s being indicative for the role of the long-living dark triplet state in the emission dynamics.

In Figure 5a, the definition of the bunching amplitude with respect to $g^{(2)}(t) = 1$ is indicated, the latter referring to the

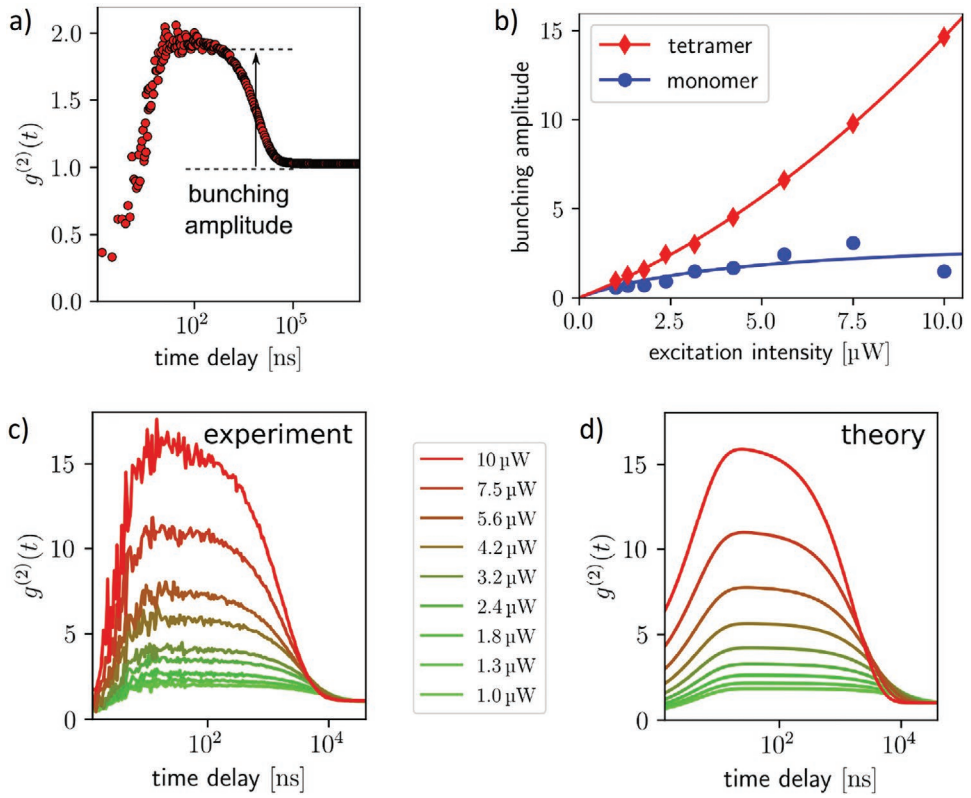

Figure 5. a) Definition of the bunching amplitude in the $g^{(2)}$ function of a single emitter at long delay times. b) Comparison of the power-dependent bunching amplitude for a PBI monomer and tetramer macrocycle. The quadratic increase of the PBI tetramer $g^{(2)}$ function with power can be related to an incremental contribution of dark states to the radiative emission of this macrocycle. Simulations of the experimental data, c) by a 4-level excitation scheme, d) yields a good agreement of the bunching amplitude in the studied power regime.

borderline case of uncorrelated photon emission within this time delay bin. Measuring the bunching height as function of excitation power, a significantly different behavior can be found for monomer versus tetramer, Figure 5b. Whereas the monomer shows a trend corresponding to that of a saturated three-level system, the power-dependent bunching height of **4PBI** raises quadratically, already hinting at an underlying two state mechanism being in charge. To access this phenomenon more quantitatively, we have modeled the experimental bunching curves (Figure 5c) at different powers. As a simple three-level scheme turned out to be not sufficient to reproduce the measured data, this scheme had to be extended by an additional level, resulting in an excellent agreement between experiment and theory (Figure 5d). Asking on the photophysical origin of this fourth level in the context of the conclusions drawn so far, the only excitation being able to rationalize the observed behavior is a doubly excited $S_1 + S_1$ singlet state. A similar state has been found in multichromophoric dendrimers based on perylene imides and can be somehow seen as an analog to biexcitonic states occurring upon excitation of inorganic quantum dots at cryogenic temperatures.[23,39] In combination with the three-level excitation scheme of the PBI monomer, the transition rates of the $S_1 + S_1$ state define the only free parameters in our 4-level model (**Figure 6**a). As the number of free parameters imposes limits on their precise estimation, we only cite the respective transition times as estimated orders of magnitude. As such, the model provides two important insights in the macrocycle excitation. At first, the doubly excited $S_1 + S_1$ state has an extremely short lifetime, mainly caused by efficient nonradiative relaxation to the S_1 state. At second, the intersystem crossing from the $S_1 + S_1$ state proceeds two orders of magnitude faster than from the S_1 state making it the predominant relaxation channel from the singlet to the triplet spin system of the macrocycle. These conclusions are corroborated by the power-dependent bunching time displayed in Figure 6b. Due to the fast intersystem crossing transition in combination with multiple triplet states and their annihilation available in the **3PBI** and **4PBI** macrocycles, the time limiting step of the slow intersystem crossing from the single S_1 state and the following relaxation to the ground state can be bypassed yielding a faster re-excitation of the macrocycle. This process is qualitatively illustrated for the monomer and the tetramer in Figure 6c. Based on the estimated transition times in our model, the probability to find a monomer in its dark triplet state at an excitation power of 100 µW is 80% whereas for the tetramer this value amounts to 96%. This situation becomes even more critical in case of electrically driving the PBI species as the triplet state can be directly populated by an injected electron and hole. While this is the main reason for using phosphorescent instead of fluorescent molecules in opto-electronic devices, at the end of our study we will evaluate whether the efficient intersystem crossing and triplet-triplet annihilation in our macrocycles can lift this fundamental constraint.

2.5. Organic Light Emitting Diodes with PBI Trimers

For this purpose, OLEDs were prepared with active matrices made of blends of poly(vinylcarbazole) (PVK), (HOMO: –5.5 eV / LUMO: –2.0 eV) and 2-*tert*-butylphenyl-5-biphenyl-1,3,4-oxadiazol (PDB) (HOMO: –6.1 eV / LUMO: –2,5 eV) and doped by PBI monomers and macrocycles at the single molecule level, respectively.[40] Regarding the band-gap of the matrix and its resulting emission in the blue at around 450 nm we exclude efficient Förster resonant energy transfer between matrix and dopants due to the small spectral overlap in this range. This is substantiated by the fact that we do not see emission in case of **1PBI** dopants which should absorb in the same spectral range

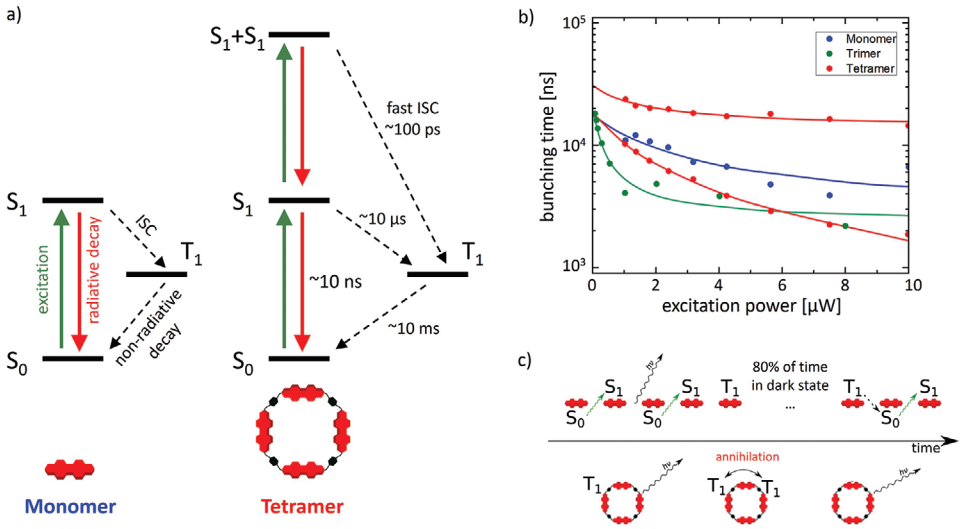

Figure 6. a) 3- and 4-level schemes explaining the observed photon correlations properties of PBI monomer and tetramer. The additional triplet relaxation channel for **4PBI** allows for a faster T_1 depopulation and, thus, shorter re-excitation cycles compared to the PBI monomer. b) Bunching time for **1PBI**, **3PBI**, and **4PBI** as function of excitation power. Here, the bunching time is shown for both tetramer configurations identified in the experiments (see the text). A decrease in bunching time with increasing power is observed for all PBI species, with a more rapid decrease for **3PBI** and **4PBI**. c) Toy model explaining qualitatively the power-dependent bunching time behavior. For monomers re-excitation is blocked by long-living triplet dark state while for multichromophores additional pathways allow for faster re-excitation with increasing power.

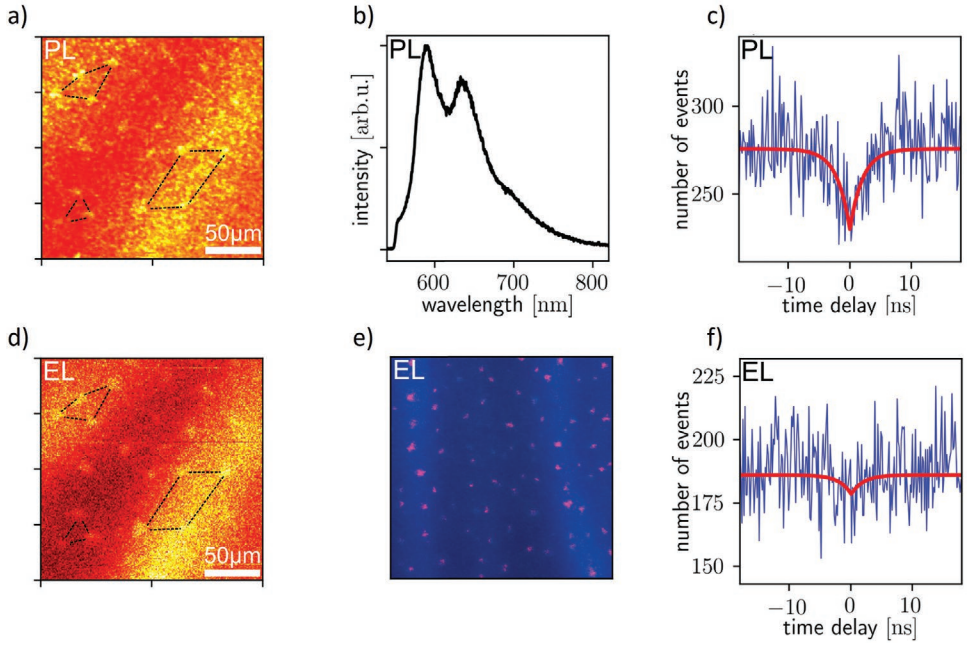

Figure 7. Organic light emitting diodes based on PVK:PBD blends doped by PBI macrocycles. a) Photoluminescence intensity map of a PBI trimer doped OLED. Dashed lines act as guidance to identify the same spots in PL and EL intensity maps. b) The corresponding spectral emission resembles that observed in solution as well as in solid PMMA. c) PL anticorrelation measured on a bright spot in a) and indicating the emission from a single molecule upon optical excitation. d) Electroluminescence map recorded on the same area and exhibiting same bright spots as in photoluminescence (a). e) Due to the brightness of the doped **3PBI** trimers, their EL is also visible under a microscope as shown in (e). f) Anticorrelation behavior under electrical excitation of the **3PBI** trimer doped OLED. The raw data (no background correction performed) shows the emergence of a dip and, thus, the tendency of antibunching at zero time delays, providing a first hint on single photon emission by electrically driven fluorescent PBI trimers at room temperature.

as the **3PBI** trimers utilized for our proof-of-concept devices discussed in the following.

Figure 7 comprises the resulting photoluminescence (PL) and electroluminescence (EL) data measured on an ITO/PEDOT:PSS/PBI-trimer:PVK:PBD/3TPYMB/Ca/Al stacked OLED device (see the Experimental Section for further information on the sample structure). In the first row, Figure 7a shows a PL intensity map at 532 nm excitation wavelength with the bright spots identified as **3PBI** species by their related emission spectra (Figure 7b). In addition, the $g^{(2)}$ antibunching clearly detectable at short delay times (Figure 7c) indicates the emission region to presumably consist of a single molecule, in accordance to the chosen dopant concentration. Operating the device at an applied voltage of 10 V, the same bright spots as before can now be identified in the EL intensity map (Figure 7d). The emission of the spots is even so bright that they can be recognized by the bare eye in a microscope as shown by the photo in Figure 7e. Finally, despite the strong contribution by the OLED background, the tendency of a dip at $g^{(2)}(0)$ can be recognized for the spot observed in Figure 7f. Although the raw data without background correction yields $g^{(2)}(0) = 0.85$ with a confidence interval of $p = 2.3\sigma$ and, thus, do not directly support single molecule emission, there are two reasons which are in favor of the latter. First and foremost, measuring the same spot under photoexcitation reveals a clear antibunching, i.e., single molecule emission behavior, as indicated in Figure 7c. Second, $g^{(2)}(0)$ dips have been observed also on other molecules within the sample, though of even weaker signal-to-noise ratio but with a tendency for antibunching at optical excitation. Often in literature, a background correction is applied by subtracting and normalizing the $g^{(2)}$ correlation function for the square of the signal-to-noise ratio, which here would result in a corrected $g^{(2)}(0)$ value of about 0.75.[12,41] However, we refrain from pursuing this correction procedure since, a priori, it is not obvious whether the background is uncorrelated with the PBI emission signal and, moreover, we observed an increase of background intensity of our OLED device over time during electrical operation. As the total measurement time of our **3PBI**-doped OLED is limited by this increase in background signal but not by photobleaching of the trimers themselves and as the latter provide intensities of around 100 cts ms^{-1}, e.g., for the spot measured in Figure 7f, we considered our proof-of-concept OLED, based on electrically driven photon emission by fluorescent emitters at room temperature, to be successful and of great potential for future optoelectronic device concepts.

3. Conclusion

In summary, we have shown that the multiple-state interplay in multichromophore perylene bisimide (PBI) trimer and tetramer macrocycles can lead to an efficient depopulation of long-living dark states and, thereby, enhanced fluorescence at strong excitation. As a result, the power-dependent fluorescence intensity scales super-linear with the number of PBI chromophores constituting the macrocycle. Yet, the distinct

antibunching in the photon-correlation measurements proves the single photon emission character of all PBI compounds caused by fast singlet-singlet annihilation on the macrocycle. In combination with the exceptional photostability, this renders PBI macrocycles potential candidates for nonclassical light sources at room temperature. Employing the efficient triplet state depopulation, usually limiting the emission of electrically driven fluorophores, we are able to demonstrate a prototypical OLED, hosting PBI trimer single molecules as emitting species and showing bright electrofluorescence of 100 cts ms^{-1} under operation at room temperature. Hence, we consider our work to constitute an important step toward a new class of opto-electronic devices utilizing multichromophore macrocycles to achieve highly efficient fluorescence under electrical operation.

4. Experimental Section

The synthesis of all PBI dyes **1PBI**, **3PBI**, and **4PBI** utilized in this study has been described in a previous work.[15]

Samples for the single molecule photon-correlation studies were prepared in a glove box under nitrogen atmosphere by spin-coating (30 s at 1500 rpm) a highly diluted solution of PBI-doped PMMA (doping concentration 10^{-8} wt%) in dichloromethane. Prior to deposition, the glass substrates of 150 µm thickness were cleaned by distilled water, acetone, and isopropanol in an ultrasonic bath and by oxygen plasma etching for 10 min. Finally, all samples were encapsulated with an additional glass slide, glued to the substrate by a low vapor pressure epoxy (TorrSeal, Kurt J. Lesker).

Prototypical OLEDs were prepared under inert nitrogen atmosphere in a glove box system. Glass supports of 150 µm thickness covered by 150 nm thick indium-tin-oxide (ITO) at a sheet resistance of 30–60 $\Omega\,\square^{-1}$ (SPI Supplies Brand) were used and precleaned by water, acetone, and isopropanol. The active ITO anode area was photo-lithographically structured into 3 mm wide stripes and cleaned, thereafter, by a 10 min oxygen plasma treatment. Next, a 40 nm thin layer of poly-3,4-ethylen dioxythiophene:polystyrene sulfonate (PEDOT:PSS, Clevios P VP AI 4083) was spin-coated (4800 rpm for 30 s) and postannealed at 135 °C for 30 min. In the following step, PBI monomers or macrocycles were added to a polyvinylcarbazole:2-tert-butylphenyl-5-biphenyl-1,3,4-oxadiazol (PVK:PBD) mixture solved at a concentration of 5 mg mL^{-1} in spectroscopic grade dichloromethane. PVK as well as PBD were purchased by Sigma-Aldrich and used without further purification. Afterward, a 100 nm thick layer of tris-[3-(3-pyridyl)mesityl]borane (3TPYMB) purchased from Merck KGaA and used without further purification was deposited on top of the PBI-doped PVK:PBD blend and acted as electron selective transport layer and injection layer. Layered cathodes composed of 20 nm Ca covered by 120 nm aluminum were thermally evaporated onto the stack via shadow masks with an active injection area of 2 mm diameter. Finally, the resulting ITO/PEDOT:PSS/PBI-doped:PVK:PBD/3TPYMB/Ca/Al structure was sealed by a glass subtracted glued by TorrSeal, Kurt J. Lesker.

Single molecule photoluminescence and photon-correlation studies were carried-out by a confocal microscope setup which allows for optical excitation by a 532 nm cw-laser of maximum 195 µW power or electrical excitation by a current–voltage source. For this purpose, the samples (thin film or OLED) were mounted on a piezo stage enabling an overall scan range of 200 × 200 μm^2. Single molecule photoluminescence was collected by a high numerical aperture immersion oil objective (100 x, NA = 1.49) which, in combination with a pin-hole (75 µm diameter), allows for ≈300 nm lateral resolution. After passing a 550 nm long-pass filter, the emitted light was spectrally analyzed by a spectrometer (Modell Acton SP2300) in combination with a CCD camera (Modell Pixis 400B). To determine the photon correlation, alternatively, two single photon avalanche diodes (Excelitas SPCM-14, QE ~ 65% at 650 nm, dark counts < 100 cts ms^{-1}) combined with a 50:50 beam splitter in a Hanbury–Brown and Twiss setup were used. The $g^{(2)}$ function of the detected photons was determined by a hardware correlation card (Becker & Hickl GmbH, DPC-230) at a time resolution below 350 ps limited by the electronic jitter of the avalanche photodiodes. For power cycled excitation of the samples, a neutral density filter wheel rotating at 4 Hz was used.

The detected anticorrelation events were modeled according to the function

$$g^{(2)}(\Delta t) = 1 - e^{-(k_{abs}+k_r+k_{nr})\Delta t} \quad (3)$$

with the absorption rate, k_{abs}, and the radiative and nonradiative emission rates, k_r and k_{nr}.[11] In case of weak excitation, i.e., $k_{abs} < k_r$ and k_{nr}, Equation (3) yields the FWHM cited in Section 2.3 above.[14,41]

Acknowledgements

The authors thank the Bavarian Ministry of Science and the Arts for the generous support by the research program Solar Technologies Go Hybrid.

Open access funding enabled and organized by Projekt DEAL.

Conflict of Interest

The authors declare no conflict of interest.

Data Availability Statement

The data that support the findings of this study are available from the corresponding author upon reasonable request.

Keywords

multichromophores, organic light emitting diodes, perylene dyes, photon-correlation, single photon emission

Received: January 31, 2022
Revised: April 5, 2022
Published online: May 29, 2022

[1] M. Knupfer, *Appl. Phys. A* **2003**, *77*, 623.
[2] T. Basché, W. E. Moerner, M. Orrit, H. Talon, *Phys. Rev. Lett.* **1992**, *69*, 1516.
[3] L. Fleury, J. -M. Segura, G. Zumofen, B. Hecht, U. P. Wild, *Phys. Rev. Lett.* **2000**, *84*, 1148.
[4] J. Lee, H. F. Chen, T. Batagoda, C. Coburn, P. I. Djurovich, M. E. Thompson, S. R. Forrest, *Nat. Mater.* **2015**, *15*, 92.
[5] C. Y. Kuei, W. L. Tsai, B. Tong, M. Jiao, W. K. Lee, Y. Chi, P. T. Chou, *Adv. Mater.* **2016**, *28*, 2795.
[6] M. C. Gather, A. Köhnen, A. Falcou, H. Becker, K. Meerholz, *Adv. Funct. Mater.* **2007**, *17*, 191.
[7] B. Lounis, M. Orrit, *Rep. Prog. Phys.* **2005**, *68*, 1129.
[8] F. Fuchs, B. Stender, M. Trupke, D. Simin, J. Pflaum, V. Dyakonov, G. V. Astakhov, *Nat. Commun.* **2015**, *6*, 7578.
[9] M. Nothaft, S. Höhla, F. Jelezko, J. Pflaum, J. Wrachtrup, *Phys. Status Solidi B* **2012**, *249*, 661.
[10] M. A. Baldo, D. F. O'Brien, Y. You, A. Shoustikov, S. Sibley, M. E. Thompson, S. R. Forrest, *Nature* **1998**, *395*, 151.

[11] D. Hu, H. P. Lu, *Phys. Chem. B* **2005**, *109*, 9861.
[12] M. Nothaft, S. Höhla, F. Jelezko, N. Frühauf, J. Pflaum, J. Wrachtrup, *Nat. Commun.* **2021**, *3*, 628.
[13] H. Uoyama, K. Goushi, K. Shizu, H. Nomura, C. Adachi, *Nature* **2021**, *492*, 234.
[14] M. Gernert, L. Balles-Wolf, F. Kerner, U. Müller, A. Schmiedel, M. Holzapfel, C. M. Marian, J. Pflaum, C. Lambert, A. Steffen, *J. Am. Chem. Soc.* **2020**, *142*, 8897.
[15] P. Spenst, R. M. Young, B. T. Phelan, M. Keller, J. Dostál, T. Brixner, M. R. Wasielewski, F. Würthner, *J. Am. Chem. Soc.* **2017**, *139*, 2014.
[16] E. Lang, F. Würthner, J. Köhler, *ChemPhysChem* **2005**, *6*, 935.
[17] A. Issac, R. Hildner, C. Hippius, F. Würthner, J. Köhler, *ACS Nano* **2014**, *8*, 1708.
[18] M. Haase, C. G. Hubner, F. Nolde, K. Müllen, T. Basché, *Phys. Chem. Chem. Phys.* **2011**, *13*, 1776.
[19] R. Metivier, F. Nolde, K. Müllen, T. Basché, *Phys. Rev. Lett.* **2007**, *98*, 047802.
[20] H. Yoo, H. W. Bahng, M. R. Wasielewski, D. Kim, *Phys. Chem. Chem. Phys.* **2012**, *14*, 2001.
[21] A. Issac, R. Hildner, D. Ernst, C. Hippius, F. Würthner, J. Köhler, *Phys. Chem. Chem. Phys.* **2012**, *14*, 10789.
[22] J. -E. Lee, V. Stepanenko, J. Yang, H. Yoo, F. Schlosser, D. Bellinger, B. Engels, I. G. Scheblykin, F. Würthner, D. Kim, *ACS Nano* **2013**, *7*, 5064.
[23] S. Masuo, T. Vosch, M. Cotlet, P. Tinnefeld, S. Habuchi, T. D. M. Bell, I. Osterling, D. Beljonne, B. Campagne, K. Müllen, M. Sauer, J. Hofkens, F. C. De Schryver, *J. Phys. Chem. B* **2004**, *108*, 16686.
[24] F. C. De Schryver, T. Vosch, M. Cotlet, M. Van der Auweraer, K. Müllen, J. Hofkens, *Acc. Chem. Res.* **2005**, *38*, 514.
[25] R. Metivier, F. Kulzer, T. Weil, K. Müllen, T. Basché, *J. Am. Chem. Soc.* **2004**, *126*, 14364.
[26] D. Wöll, E. Braeken, A. Deres, F. C. De Schryver, H. Uji-i, J. Hofkens, *Chem. Soc. Rev.* **2009**, *38*, 313.
[27] M. Sliwa, C. Flors, I. Oesterling, J. Hotta, K. Mülen, F. C. De Schryver, J. Hofkens, *J. Phys.: Condens. Matter* **2007**, *19*, 445004.
[28] P. Dodecker, B. Muls, A. Deres, H. Uji-i, J. Hotta, M. Sliwa, J. P. Soumillion, K. Müllen, J. Enderlein, J. Hofkens, *Adv. Mater.* **2009**, *21*, 1079.
[29] P. Leowanawat, A. Nowak-Król, F. Würthner, *Org. Chem. Front.* **2016**, *3*, 537.
[30] A. Nowak-Król, F. Würthner, *Org. Chem. Front.* **2019**, *6*, 1272.
[31] F. Würthner, *Pure Appl. Chem.* **2006**, *78*, 2341.
[32] F. Schlosser, J. Sung, P. Kim, D. Kim, F. Würthner, *Chem. Sci.* **2012**, *3*, 2778.
[33] P. Spenst, F. Würthner, *Angew. Chem.* **2015**, *127*, 10303; *Angew. Chem., Int. Ed.* **2015**, *54*, 10165.
[34] P. Spenst, R. M. Young, M. R. Wasielewski, F. Würthner, *Chem. Sci.* **2016**, *7*, 5428.
[35] P. Osswald, F. Würthner, *Chem. - Eur. J.* **2007**, *13*, 7395.
[36] We would like to point out that a second series of PBI tetramers with distinctly different optical properties in respect to spectral emission has been identified in the single molecule experiments which we related to the possible dimer configuration reported also in ref. [20]. However, due to pronounced fluctuations in the emission spectra and intensity, in particular, at higher excitation power we were not able to deduce reliable photon statistics on this kind of PBI multi-chromophore and, hence, did not consider it in the further analyses.
[37] T. Brixner, R. Hildner, J. Köhler, C. Lambert, F. Würthner, *Adv. Energy Mater.* **2017**, *7*, 1700236.
[38] W. E. Moerner, *Science* **1997**, *277*, 1059.
[39] G. Bacher, R. Weigand, J. Seufert, V. D. Kulakovskii, N. A. Gippius, A. Forchel, K. Leonardi, D. Hommel, *Phys. Rev. Lett.* **1999**, *83*, 4417.
[40] C. C. Wu, J. C. Sturm, R. A. Register, J. Tian, E. P. Dana, M. E. Thompson, *IEEE Trans. Electron Devices* **1997**, *44*, 1269.
[41] J. Bernard, L. Fleury, H. Talon, M. Orrit, *J. Chem. Phys.* **1993**, *98*, 850.